Papers

Phase Conjugate Optics and Real-Time Holography

AMNON YARIV, FELLOW, IEEE

(*Invited Paper*)

Abstract—**Nonlinear optical mixing can be used to perform a variety of new optical functions, as well as real-time holography. The theory and some of the first experiments are described.**

I. Introduction

PHASE conjugate optics (PCO) is the name which seems to attach itself to a new and exciting area in coherent optics. This area involves the use of *nonlinear optical techniques* for *real-time processing of electromagnetic fields*. The name, phase conjugate optics, is due to the fact that all the applications demonstrated or proposed to date involve phase reversal of an incoming electromagnetic wave.

The field is still young enough so that a brief recounting of the main developments is possible. The first milestone was the demonstration by Zeldovich, Nosach, and collaborators [1], [2] of the cancellation of propagation distortion by stimulated Brillouin scattering. The author, independently, proposed [3], [4] and analyzed the use of three-wave mixing in crystals for overcoming image "loss" by modal phase dispersion in multimode fibers and for real-time holography. Hellwarth suggested [5] four-wave mixing as an attractive process for phase conjugation, and showed that it overcomes some serious phase matching problems inherent in three-wave processes. Yariv and Pepper [6] showed that the four-wave process for phase conjugation was also capable of amplifying an incoming wave, as well as rendering its complex conjugate version and, in the limit of sufficient pumping, of mirrorless oscillation.

The first observations of phase conjugation by four-wave mixing were reported by Jensen and Hellwarth [7] and by Bloom and Bjorklund [8], both parties using CS_2 as the nonlinear medium. Parametric amplification and oscillation in four-wave mixing was reported by Bloom, Liao, and Economou [9] and by Pepper, Fekete, and Yariv [10]. Phase conjugation by three-wave mixing in crystals was demonstrated by Avizonis *et al.* [11]. Wang and Guiliano [12] demonstrated the ability of the stimulated Brillouin process to restore high spatial frequencies. Optical phase conjugation and image restoration by stimulated Raman scattering was demonstrated by Zeldovich and collaborators [13].

Manuscript received May 3, 1978. This work was supported by the Army Research Office, Durham, NC.

The author is with the Departments of Applied Physics and Electrical Engineering, California Institute of Technology, Pasadena, CA 91125.

II. Phase Conjugation as "Time Reversal"

Before embarking on a detailed discussion of the means for obtaining complex conjugates of electromagnetic fields, it may be useful to describe the properties of such fields. We will do so in two different instances: (A) propagation through a distorting medium; and (B) image transmission in a fiber.

A. Propagation through a Distorting Medium

Consider as an example the problem of an optical beam

$$E_1(\vec{r}, t) = \text{Re}\,[\psi(\vec{r}) \exp i(\omega t - kz)] = \text{Re}\,[A_1(\vec{r})\, e^{i\omega t}] \tag{1}$$

propagating through a linear lossless distorting medium essentially in the z direction (from left to right). The dependence of ψ on $\vec{r}$ reflects spatial modulation by information, the effects of distortion, and diffraction. If in some region of space near z_0 we somehow generate a field $E_2(\vec{r}, t)$ which, locally, is described by

$$E_2(\vec{r}, t) = \text{Re}\,[\psi^*(\vec{r}) \exp i(\omega t + kz)] = \text{Re}\,[A_2(\vec{r})\, e^{i\omega t}] \tag{2}$$

then

$$A_2(\vec{r}) = A_1^*(\vec{r}) \text{ for all } z < z_0.$$

The field $E_2(\vec{r}, t)$ will be called in this paper the *complex conjugate* of $E_1(\vec{r}, t)$. We note that to get E_2 from E_1 we take the complex conjugate of the *spatial part only*, leaving the factor $\exp(i\omega t)$ intact. (This is equivalent to leaving the spatial part alone but reversing the sign of t. That is, the field E_2 is related to E_1 by "time reversal.")

To appreciate the practical consequences of conjugation, consider a field E_1 propagating from left to right through a distorting medium. This causes the wave to "lose" whatever

0018-9197/78/0900-0650$00.75

information it may carry as spatial modulation or to acquire some undesirable spatial properties. If the complex conjugate field E_2 is generated, it will traverse the distorting medium in the reverse direction and reemerge with the original unspoiled properties of the beam E_1.

The above statements can be verified by considering the propagation of an optical beam

$$E_1(\vec{r}, t) = \text{Re}\ [\psi(\vec{r}) \exp i(\omega t - kz)] \tag{3}$$

propagating from left to right through an "atmosphere" whose dielectric constant, assumed stationary over the time needed for a round trip, is $\epsilon(\vec{r})$. (The medium is assumed lossless, so $\epsilon(r)$ is real.)

The (scalar) wave equation is taken as

$$\nabla^2 E + \omega^2 \mu \epsilon(\vec{r})\, E = 0,$$

which, using (3) becomes

$$\nabla^2 \psi + [\omega^2 \mu \epsilon(\vec{r}) - k^2]\ \psi - 2ik \frac{\partial \psi}{\partial z} = 0.$$

The complex conjugate of the last equation

$$\cdot \nabla^2 \psi^* + [\omega^2 \mu \epsilon(\vec{r}) - k^2]\ \psi^* + 2ik \frac{\partial \psi^*}{\partial z} = 0 \tag{4}$$

can be viewed formally as the wave equation describing the propagation of

$$E_2(\vec{r}, t) = \text{Re}\ [\psi^*(\vec{r}) \exp i(\omega t + kz)]$$

which is a wave propagating in the $(-z)$ direction, i.e., oppositely to $E_1(\vec{r}, t)$ and having at *each point* a complex amplitude equal to the complex conjugate of E_1. This one-to-one correspondence between the two waves is the reason for the unraveling of the degradation effects (equivalent to time reversal) in the propagation of the conjugate beam.

The "healing" of spatial distortion by generating a complex conjugate wave and having it propagate backwards through a distorting medium is demonstrated by Fig. 1, which shows the difference between a conventional reflection and "conjugate" reflection. The key point to appreciate is that a "conjugate mirror" yields reflected wavefronts that are identical to those of the incident ones. In conventional mirrors, on the other hand, the two sets of wavefronts are related by reflection.

B. Image Transmission in Fibers

The second fundamental illustration of the potential area of application of phase conjugation is in long distance image transmission in optical waveguides. The problem of phase conjugation in an optical waveguide, say a fiber, is illustrated in Fig. 2. Let the incident field at the input plane of the guide be

$$f_1(x, y, z = 0, t) = \sum_{m=0}^{N} \sum_{m=0}^{N} A_{mn} E_{mn}(x, y) \exp\ [i(\omega t)] \tag{5}$$

where E_{mn} is the spatial mode function m, n of the particular waveguide used. The summation is over the discrete spectrum of guided modes whose number is taken as N^2. The output field at the fiber's end is obtained by propagating each mode a distance L, and then summing up

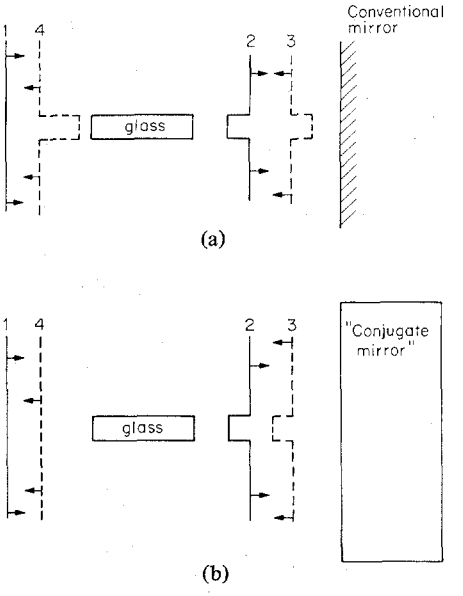

Fig. 1. (a) A plane wave (1) is incident on a distorting element (a glass cylinder) emerging with a bulge (2). The wave reflected from a conventional mirror (3) traverses the cylinder in reverse, resulting in a doubling of the bulge depth. (b) A conjugate mirror yields a reflected wavefront (3) which is identical to the incident wave (2). The result is a perfect smoothing of the bulge in (4), so that (4) and (1) are identical.

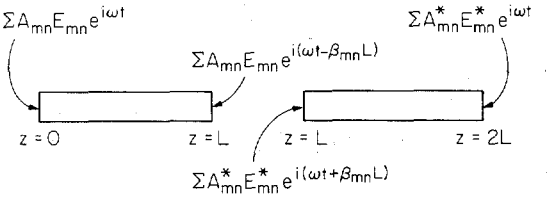

Fig. 2. Compensation (and restoration) for image loss by modal dispersion in a dielectric waveguide using phase conjugation.

$$f_2(x, y, L, t) = \sum_m \sum_n A_{mn} E_{mn}(x, y) \exp\ [i(\omega t - \beta_{mn} L)] \tag{6}$$

where β_{mn} is the propagation constant of mode m, n and where we have neglected the possibility of mode dependent losses. In general, the picture field (6) is different from the input field (5), due to the phase factors $\beta_{mn}L$. In practice, this corresponds to a scrambling of spatial information. If, however, we can generate a complex conjugate of the output field (6)

$$f_3(x, y, L, t) = \sum_m \sum_n A^*_{mn} E^*_{mn}(x, y) \exp\ [i(\omega t + \beta_{mn} L)] \tag{7}$$

and launch it into a section of length L of a fiber identical in length and all other characteristics to the first one, the result would be an output field

$$\begin{aligned} f_4(x, y, 2L, t) &= \sum_m \sum_n A^*_{mn} E^*_{mn}(x, y) \\ &\quad \cdot \exp\ [i(\omega t + \beta_{mn} L - \beta_{mn} L)] \\ &= \sum_m \sum_n A^*_{mn} E^*_{mn}(x, y) \exp\ (i\omega t). \end{aligned} \tag{8}$$

Except for the complex conjugation, the field at $z = 2L$, f_4 is the same as the input field f_1 and the spatial information carried by the wave has thus been recovered.

Next we will discuss the basic approaches proposed to date for phase conjugation.

III. Wave Conjugation by Three-Wave Mixing

Three-wave mixing of optical waves takes place in crystals lacking inversion symmetry [14]. If two fields

$$E_1 = \tfrac{1}{2}A_1 \exp i(\omega t - k^{\omega} z) + \text{c.c.}$$

and (9)

$$E_2 = \tfrac{1}{2}A_2 \exp i(2\omega t - k^{2\omega} z) + \text{c.c.}$$

are incident on such a crystal, then a polarization will be set in the crystal in the form of

$$\begin{aligned} P^{(NL)}_{(z,t)} &= \tfrac{1}{2}dA_2 \exp i(2\omega t - k^{2\omega} z) \\ &\quad \cdot [E_1 \exp i(\omega t - k^{\omega} z)]^* + \text{c.c.} \\ &= \tfrac{1}{2}dA_2 A_1^* \exp i[\omega t - (k^{2\omega} - k^{\omega})z] + \text{c.c.} \end{aligned} \tag{10}$$

If $k^{2\omega} = 2k^{\omega}$, the polarization $P^{(NL)}$ will radiate a wave

$$E_3 \propto dA_2 A_1^* \exp i(\omega t - k^{\omega} z) \tag{11}$$

which, upon conventional reflection from a plane mirror, becomes

$$(E_3)_{\text{refl}} \propto dA_2 A_1^* \exp i(\omega t + k^{\omega} z) \tag{12}$$

and is thus the complex conjugate of the original field E_1.

The use of three-wave mixing plus conventional reflection for phase conjugation is demonstrated in Fig. 3.

The basic disadvantage of three-wave phase conjugation is the fact that for efficient generation of the conjugate field, the phase matching condition

$$k^{2\omega} = 2k^{\omega} \tag{13}$$

need be satisfied [14]. In a crystal this condition can be satisfied exactly along one direction only. This causes a serious limitation on the angular divergence of the input beam, and hence on the amount of information or distortion which can be conjugated or corrected. This problem is discussed in some detail in [4] and [11], which describes the experimental demonstration of phase conjugation in three-wave mixing.

IV. Theory of Phase Conjugation by Four-Wave Mixing

Four-wave mixing for phase conjugation has been proposed by Hellwarth [5]. The possibility of using this effect for wave amplification and oscillation as well as conjugation has been pointed out by Pepper and Yariv [6]. We shall outline in what follows, the basic theoretical background of these ideas and also describe some of the experiments performed to date.

The basic experimental arrangement of four-wave mixing is shown in Fig. 4. A nonlinear medium characterized by a third-order nonlinear polarization

$$P^{(NL)}(\omega_3 = \omega_1 + \omega_2 - \omega_4) = \chi^{(3)} A_1^{(\omega_1)} A_2^{(\omega_2)} A_4^{*(-\omega_4)} \tag{14}$$

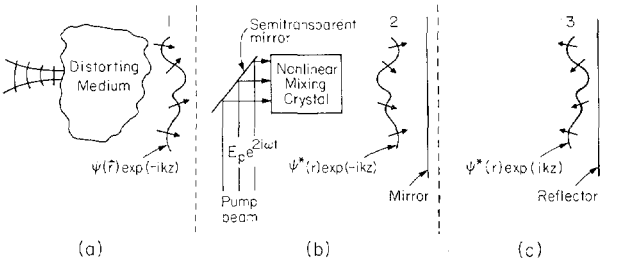

Fig. 3. Complex conjugation of an input field $\psi(\vec{r})$ exp $(-ikz)$ at (a) is achieved by difference frequency "mixing" in a nonlinear crystal (b) followed by reflection (c) from a conventional mirror.

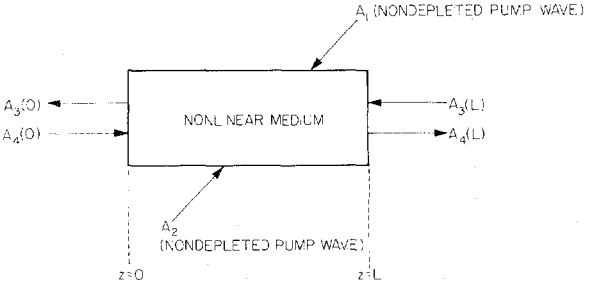

Fig. 4. Four-wave mixing geometry (assuming nondepleting pump waves).

is used to mix input waves A_1, A_2, and A_4 defined by

$$E_i(\vec{r}, t) = \tfrac{1}{2}A_i(r_i) \exp i(\omega_i t - \vec{k}_i r) + \text{c.c.} \tag{15}$$

Waves 1 and 2 are chosen so as to travel in exact opposition to each other and are of the same frequency so that

$$\vec{k}_1 + \vec{k}_2 = 0. \tag{16}$$

Wave 4, also at ω, is incident along an arbitrary direction which is designated as z. The induced nonlinear polarization [14] is thus of the form

$$\begin{aligned} P^{(NL)}(\omega = \omega + \omega - \omega) &= \tfrac{1}{2}\chi^{(3)} A_1 A_2 A_4^* \\ &\quad \cdot \exp i[(\omega + \omega - \omega)t \\ &\quad - (\vec{k}_1 + k_2)\vec{r} + kz] + \text{c.c.} \\ &= \tfrac{1}{2}\chi^{(3)} A_1 A_2 A_4^* \\ &\quad \cdot \exp i(\omega t + kz) + \text{c.c.} \end{aligned} \tag{17}$$

and causes a fourth wave at ω traveling in the $-z$ direction to be generated. This wave is proportional according to (17) to A_4^* and is thus the desired complex conjugate.

In the analysis of this effect we start with the wave equation (CGS units)

$$\vec{\nabla} \times \vec{\nabla} \times \vec{E} + \frac{\epsilon}{c^2}\frac{\partial^2 E}{\partial t^2} = \frac{4\pi}{c^2}\frac{\partial^2}{\partial t^2}\vec{P}^{(NL)} \tag{18}$$

and after applying the standard methods of nonlinear optics [14] obtain

$$\begin{aligned} \frac{dA_3}{dz} &= i\frac{2\pi\omega}{cn}\chi^{(3)} A_1 A_2 A_4^* \exp[-i(\vec{k}_1 + \vec{k}_2 - \vec{k}_3 - \vec{k}_4)\cdot\vec{r}] \\ &= i\kappa^* A_4^* \\ \frac{dA_4^*}{dz} &= i\kappa A_3 \end{aligned} \tag{19}$$

where we used the fact that $\vec{k}_1 + \vec{k}_2 = 0$, $\vec{k}_3 + \vec{k}_4 = 0$, took the z direction as that of $\vec{k}_4$, and used the adiabatic approximation

$$\left|\frac{d^2A_i}{dz^2}\right| << \left|k_i \frac{dA_i}{dz}\right|.$$

The complex coupling constant κ is given by

$$\kappa^* = \frac{2\pi\omega}{cn}\chi^{(3)}A_1A_2. \tag{20}$$

If we specify the complex amplitudes $A_3(L)$ and $A_4(0)$ of the two weak waves at their respective input planes ($z = L$, $z = 0$), the solution of (19) is

$$A_3(z) = \frac{\cos|\kappa|z}{\cos|\kappa|L}A_3(L) + i\frac{\kappa^* \sin|\kappa|(z-L)}{|\kappa|\cos|\kappa|L}A_4^*(0)$$

$$A_4(z) = -i\frac{|\kappa|\sin|\kappa|z}{\kappa\cos|\kappa|L}A_3^*(L) + \frac{\cos|\kappa|(z-L)}{\cos|\kappa|L}A_4(0). \tag{21}$$

In the case of phase conjugation, we have a single input $A_4(0)$ at $z = 0$ and $A_3(L) = 0$. In this case, the reflected wave at the input ($z = 0$) is

$$A_3(0) = -i\left(\frac{\kappa^*}{|\kappa|}\tan|\kappa|L\right)A_4^*(0), \tag{22}$$

while at the output ($z = L$),

$$A_4(L) = \frac{A_4(0)}{\cos|\kappa|L}. \tag{23}$$

Equation (22) is our main result. It shows that at $z = 0$ the reflected field $A_3(0)$ is proportional to the complex conjugate of the incident field $A_4(0)$ multiplied by a factor $-i((\kappa^*/|\kappa|)\cdot\tan|\kappa L|)$.

The field distribution inside the interaction region for a value of κL satisfying

$$\frac{\pi}{4} < |\kappa|L < 3\pi/4 \tag{24}$$

is shown in Fig. 5. In this regime, the reflected wave intensity exceeds that of the input wave and the device functions as both a phase-conjugate-reflection and transmission amplifier.

When

$$|\kappa|L = \pi/2 \tag{25}$$

$$\frac{A_3(0)}{A_4(0)} = \infty, \quad \frac{A_4(L)}{A_4(0)} = \infty \tag{26}$$

which corresponds to oscillation. The four-wave mixing process, in analogy to a backward parametric oscillator [15] is capable of oscillation without mirror feedback.

The field distribution at the oscillation condition is illustrated in Fig. 6.

A fundamental difference between the three-wave mixing process described in Section III and the four-wave process described here is that the former depends on phase matching and the latter does not (note that the sum $\vec{k}_1 + \vec{k}_2 - \vec{k}_2 - \vec{k}_4$ in the exponents of (19) is identically zero). Because of its freedom from the need for phase matching, the four-wave phase mixing process can be used to amplify wavefronts of essentially *arbitrary complexity*.

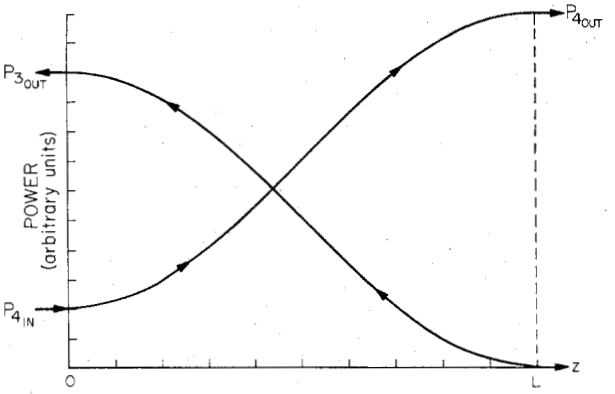

Fig. 5. Amplification by four-wave mixing. The transmission gain is $A_4(L)/A_4(0)$.

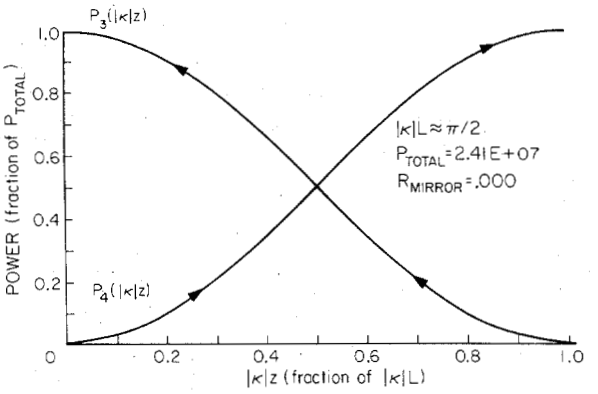

Fig. 6. The field distribution inside the interaction region when the oscillation condition $|\kappa|L = \pi/2$ is satisfied.

For the formal proof of this last statement, we Fourier expand an arbitrary input field A_4 as

$$A_4(x,y,z) = \int A_4(\vec{k}_\perp, z)\exp i\vec{k}_\perp\cdot\vec{r}_\perp\, d^2\vec{k}_\perp \exp(-ikz)$$

$$= \int A_4(-\vec{k}_\perp, z)\exp -i\vec{k}_\perp\cdot\vec{r}_\perp\, d^2k_\perp \exp(-ikz) \tag{27}$$

while the reflected output field is taken as

$$A_3(x,y,z) = \int A_3(\vec{k}_\perp, z)\exp i\vec{k}_\perp\cdot\vec{r}\, d^2\vec{k}_\perp \exp(-ikz). \tag{28}$$

Choosing the pump beams A_1 and A_2 as plane waves traveling in opposition to each other along the same arbitrary direction, we obtain by substituting (27) and (28) in the wave equation (18), and after some rearrangement:

$$\frac{\partial}{\partial z}A_3(\vec{k}_\perp, z) = -i\frac{\lambda k_\perp^2}{4\pi}A_3(\vec{k}_\perp, z) + i\kappa^* A_4^*(-\vec{k}_\perp, z),$$

$$\frac{\partial}{\partial z}A_4^*(-\vec{k}_\perp, z) = -i\frac{\lambda k_\perp^2}{4\pi}A_4^*(-\vec{k}_\perp, z) + i\kappa A_3(\vec{k}_\perp, z) \tag{29}$$

where κ is given by (20) and $k = (\omega/c)n$.

A specified input phase front at $z = 0$ amounts to specifying

$A_4^*(-\vec{k}_\perp, 0)$. Since no mixing takes place at $z > L$, we take the reflected field $A_3(\vec{k}_\perp, L)$ to be zero at the output $z = L$. With these boundary conditions, the solution to (29) is

$$A_3(\vec{k}_\perp, z) = ie^{i(k-\lambda k_\perp^2/4\pi)z}\left(\frac{\kappa^*}{|\kappa|}\right)\frac{A_4(-\vec{k}_\perp, 0)}{\cos|\kappa|L}\sin|\kappa|(z-L),$$

$$A_4^*(-\vec{k}_\perp, z) = e^{i(k-\lambda k_\perp^2/4\pi)z}A_4^*(-\vec{k}_\perp, 0)\frac{\cos|\kappa|(z-L)}{\cos|\kappa|L}. \quad (30)$$

At the input to the nonlinear medium, $z = 0$, we thus have

$$A_3(\vec{k}_\perp, 0) = -i\left(\frac{\kappa^*}{|\kappa|}\tan|\kappa|L\right)A_4^*(-\vec{k}_\perp, 0) \quad (31)$$

which shows that the individual plane wave components of the *arbitrary* wavefronts behave as in the plane wave case except that each $\vec{k}_\perp$ component of the output beam A_3 couples directly to the $-\vec{k}_\perp$ component of the input wave A_4. It is now a straightforward, though formal, procedure to show, using the uniqueness property of linear parabolic differential equations, that the relation (31) in conjunction with (19) and (28) signifies

$$A_3(x, y, z < 0) = -i\left[\left(\frac{\kappa^*}{|\kappa|}\tan|\kappa|L\right)\right]A_4^*(x, y, z < 0) \quad (32a)$$

so that an *arbitrarily complex* incident wavefront A_4 gives rise at $z < 0$ to a reflected and amplified field A_3, which is everywhere the *complex conjugate* of A_4.

We have shown above that oscillation results when $|\kappa|L = \pi/2$. This condition is most likely to be satisfied when the waves A_3 and A_4 are parallel to the input waves A_1 and A_2, since this is the direction of maximum beam overlap. This, however, is often the direction of least interest, since the "output" waves A_3 and A_4 will be degenerate in their directions, as well as their frequencies, with the "pump" waves A_1 and A_2.

To solve this problem we may add a single reflector along some *arbitrary* direction, as shown in Fig. 7. It follows directly from (21) and the boundary condition imposed by the mirror that the oscillation condition in (25) is now replaced by

$$|\kappa|L = \tan^{-1}(1/|r|) \quad (32b)$$

where $|r|^2$ is the reflectivity of the mirror. For a mirror with near-unity reflectivity, oscillation occurs at $|\kappa|L = \pi/4$, which is lower by a factor of 2 than that of the no-mirror case. The presence of an external mirror thus defines the path of lowest threshold.

V. Experiments in Four-Wave Mixing

The observation of phase conjugation by four-wave mixing was reported by Jensen and Hellwarth [7] and by Bloom and collaborators [8]. The latter group succeeded in demonstrating the existence of amplification in quantitative agreement with the theory [9]. In this section, I will describe some of the experiments performed at Caltech by D. M. Pepper, D. Fekete, and the author, which demonstrated phase conjugation, amplification, as well as oscillation in degenerate four-wave mixing [10].

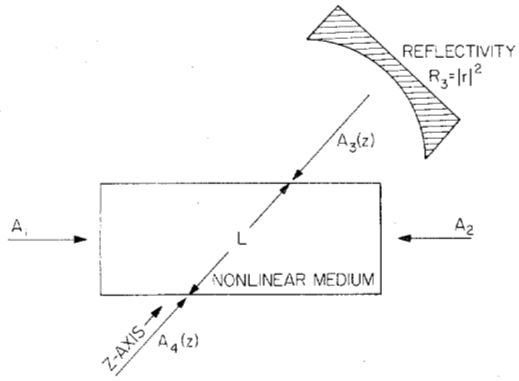

Fig. 7. Four-wave mixing utilizing external mirror of reflectivity R_3, which provides preferred direction for oscillation.

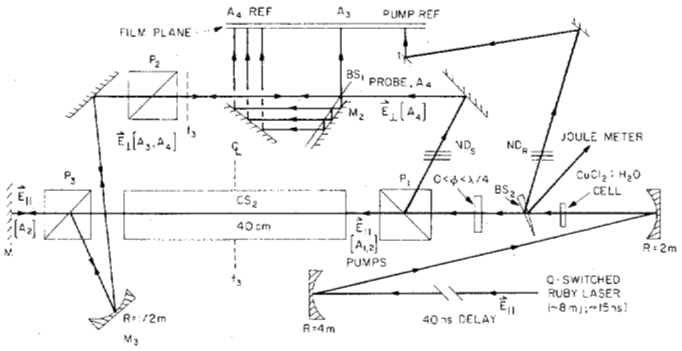

Fig. 8. Experimental apparatus for measurement of the nonlinear reflection coefficient (all mirrors are totally reflecting).

The experimental arrangement is shown in Fig. 8. Stripped of details, which will be discussed below, it consists of a CS_2 cell which is pumped simultaneously by laser beams A_1 and A_2 of the same frequency ω polarized in the plane of the figure (parallel, π-polarization) and which travel in opposition to each other. Simultaneously, an orthogonally polarized probe beam A_4 at ω is introduced from the left and travels in a direction parallel to that of A_1. What makes it possible to perform the experiment using a collinear geometry for all four waves is the existence of a nonlinear coupling described by [14]

$$P_{3y}^{(\omega_3=\omega_1+\omega_2-\omega_4)} = \chi_{yxxy}^{(3)}A_{1x}^{(\omega_1=\omega)}A_{2x}^{(\omega_2=\omega)}A_{4y}^{*(-\omega_4=-\omega)} \quad (33)$$

which couples "pump" beams A_1 and A_2 polarized along x and the input and output waves (A_4 and A_3) polarized along y. The pump and signal waves can then be separated using polarizers. In CS_2

$$\chi_{yxxy}^{(3)}/\chi_{xxxx}^{(3)} = 0.706$$

so that the use of orthogonal polarization does not entail a large sacrifice in interaction efficiency. The employment of a collinear geometry for both the signal (A_3, A_4) and pump (A_1, A_2) makes it possible to use very long interaction paths ($\geq$40 cm) and thus realize high gains and even oscillation. The pump source in the measurement of the reflection coefficient was a passively Q-switched ruby laser, operating in both a single longitudinal and transverse mode. A typical output

pulse energy was 7 to 13 mJ with a duration of 15 ns. The typical intensity spot size was determined to be 2.2 mm in diameter. The output beam was reflected by a 2:1 spherical mirror collimator and folded to yield an optical path delay of 40 ns before entering the interaction region. Thus, return signals were prevented from reaching the laser throughout the duration of the pulse. A 1 cm thick cell containing varying concentrations of $CuCl_2$ in H_2O was used to attenuate the laser beam for various input energies. The beam passed next through a calcite Glan laser prism (P_1), and then into the CS_2 medium, which was contained in a 40 cm long, 2 cm diameter glass cell. Mirror M_1 retroreflected the pump beam, giving rise to a counterpropagating component A_2. The cell was tilted off axis to prevent Fresnel reflections from interfering with measured fields. Prism P_1 served a dual function: it passed the pump beam (A_1) π-polarized into the interaction medium, and in addition coupled an "s" polarized probe A_4 pulse of order 10^{-3} that of the pump energy (energy determined by the orientation of wave plate ϕ). This probe was then beam-split and passed through a calibrated beam splitter-mirror system (BS_1, M_2) providing a sequence of reflected beams, each being reduced in intensity by a factor of two which were incident upon the film plane. For comparison, a Fresnel reflected (via BS_2) pump beam was also recorded. Both of these beams were attenuated through neutral density stacks (ND_S and ND_R) prior to impinging on the film plane. The laser energy was monitored by a calibrated Fresnel reflection (off BS_2) using a pyroelectric detector and a digital readout.

The forward-going probe beam A_4, now propagated through prism P_2, oriented to pass this s polarized field, thus serving to eliminate any scattered or Fresnel reflected π-polarized fields from creating systematics, was then coupled back into the CS_2 cell through a spherical mirror M_3 and another Glan laser prism P_3 (oriented similar to that of P_1) between the cell and M_1. Thus, prisms P_1 and P_3 constrained the probe beam to interact only in the CS_2 cell. The purpose of M_3 was to focus and confine the probe to propagate within the pump beam volume.

The phase conjugate nature of the reflected wave, i.e., $A_3(0) \propto A_4^*(0)$, was established through the use of the mirror M_3 (see Fig. 8). This mirror focuses the collimated input probe beam A_4 on the midplane f_3. A phase conjugate reflection A_3, being a "time-reversed" replica of the input wave A_4, should emerge from the CS_2 cell with virtual emanation from the focal spot at f_3 and thus be collimated. That this was the case was established using the beam spot photographs (taken by reflecting A_3 off BS_1) in the film plane.

The presence of mirror M_3 insures that only reflected phase conjugated radiation is collimated in the film plane. The presence of unwanted s-polarized radiation due to residual birefringence in the optical components, imperfect extinction in the polarizers, and to ellipse rotation in CS_2, gave rise to a divergent output and did not affect the measurement of the reflection coefficient materially.

Fig. 9 shows the measured reflection coefficient as a function of the pumping pulse energy. We note that for energies exceeding 11 mJ, the reflection coefficient exceeds unity. Also plotted in Fig. 9 is a least square fit of the function

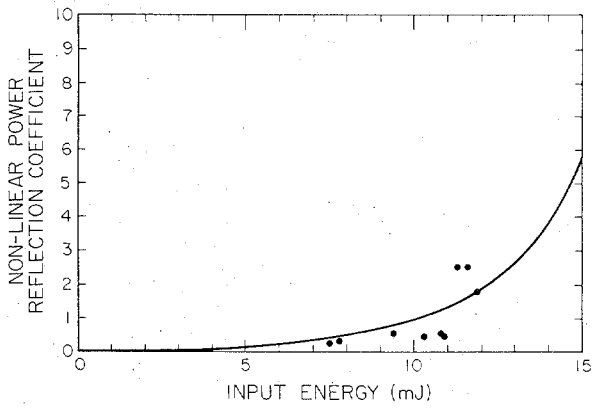

Fig. 9. Plot of nonlinear power reflection coefficient versus pump energy (in mJ). Data [•]; least squares fit to $R = \tan^2(\alpha\epsilon_p)$ [solid line].

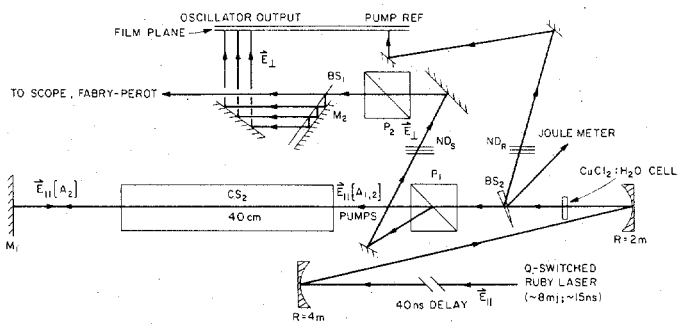

Fig. 10. Experimental apparatus for viewing oscillation.

$$R = \tan^2(\alpha\epsilon_p)$$

which is in the form predicted by (22). The value of α thus determined is employed, using (22), to calculate the value of $\chi^{(3)}_{yxxy}$ of CS_2. The result is

$$\chi^{(3)}_{yxxy} = (1.64^{+0.14}_{-0.20}) \times 10^{-12} \text{ ESU}$$

compared with a generally accepted value of $\chi^{(3)} \sim 1.8 \times 10^{-12}$ ESU. This check serves to reassure us that the observed reflection is due to the four-wave mixing process described by (22).

Self-oscillation was observed using the apparatus shown in Fig. 10. The difference between the two experimental geometries is two-fold. First, prism P_1 is used to couple out any oscillation ("s" polarized) signal, while passing the pump beams. Second, the absence of prism P_3 now allows the totally reflecting flat mirror M_1 to serve a dual function: (1) it retroreflects the pump beam (A_1), thus providing for its counterpropagating component (A_2); and (2) M_1 serves as a reflector for the orthogonally polarized oscillation field. According to (32b) for $|r| \simeq 1$, the presence of a reflector reduces the oscillation threshold by a factor of 2.

At pumping intensities exceeding 8.8 mW/cm^2 and with no input field ($A_4(0) = 0$), an intense *oscillation* pulse with orthogonal (s) polarization resulted. The oscillation pulse energy was approximately 1 percent of the pump energy. It was noted that the spot size of the oscillation beam was smaller than that of the input pump beam. This is due to the fact that the coupling constant κ in (20) is proportional to the product of two beams, A_1 and A_2, each with a Gaussian intensity profile.

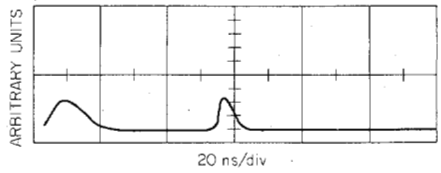

Fig. 11. Time evolution of pump (left) and oscillator (right) outputs.

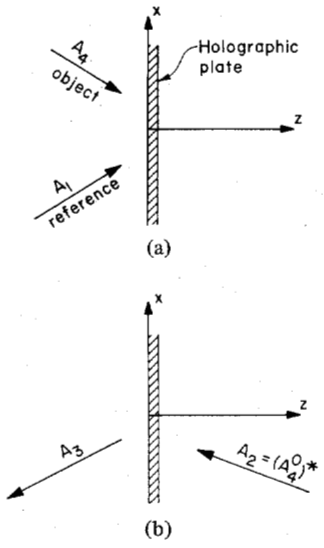

Fig. 12. A holographic exposure and reconstruction.

A typical set of temporal pulse shapes is shown in Fig. 11. The first pulse is the laser output, while the second pulse (properly delayed and of arbitrary amplitude) is the output due to the oscillation. The nonlinearity of the interaction is also evident from these data. Since the nonlinear gain requires the temporal overlap of the pump beams, the evolution of the gain in the time domain is essentially the temporal convolution of the two Gaussian pulses. This results in a nonlinear gain with a sharper and shorter Gaussian temporal characteristic. Fabry-Perot spectra of these signals verified the degenerate frequency nature of the oscillation output.

VI. Phase Conjugation as Real-Time Holography [16]

In Section I, we mentioned the holographic implications of phase conjugation. Let us elaborate on this idea at some length. We will start by discussing the formal analogy between four-wave mixing and conventional holography.

Consider the procedure of hologram recording and reconstruction as shown in Fig. 12. The first step [Fig. 12(a)] shows the recording of a thin hologram using an interference between a "reference" beam A_1 and a "signal" beam A_4. The resulting transmission function is

$$T \propto (A_4 + A_1)(A_4^* + A_1^*) = |A_4|^2 + |A_1|^2 + A_4 A_1^* + A_1 A_4^*. \tag{34}$$

$A_1(x,y)$ and $A_4(x,y)$ denote the complex amplitudes of the reference and object fields, respectively, in the hologram plane $z = 0$.

In the reconstruction step, the hologram is illuminated by a single reference wave A_2 impinging from the right in a direction opposite to that of A_1 as shown in Fig. 12(b). We thus have $A_2 = A_1^*$ so that the diffracted field to the left of the hologram is

$$\begin{aligned} A_3 = TA_2 &\propto (|A_4|^2 + |A_1|^2 + A_4 A_1^* + A_4^* A_1) A_1^* \\ &= (|A_4|^2 + |A_1|^2) A_1^* + (A_1^*)^2 A_4 + |A_1|^2 A_4^*. \end{aligned} \tag{35}$$

The first term on the right side of (35) is proportional to the incident field $A_2 (= A_1^*)$ and is of no interest in this paper. The term $(A_1^*)^2 A_4$ will, in a thick hologram, have a phase factor $\exp[-i(2\vec{k}_1 - \vec{k}_4)\cdot\vec{r}]$ and is thus phase mismatched, i.e., will not radiate. The term of interest is

$$A_3 \propto |A_1|^2 A_4^* = |A_1 A_2| A_4^* \tag{36}$$

which at $z < 0$ corresponds to a "time-reversed" phase conjugate replica of the original object field A_4. Relation (36) derived in the case of conventional holography is to be compared with that of four-wave mixing. For $|\kappa L| \ll 1$ (weak "hologram") we may rewrite (22) as

$$\begin{aligned} A_3(0) &= -i(\kappa^* L) A_4^*(0) \\ &\propto A_1 A_2 A_4^*(0) \end{aligned}$$

which is of a form identical to (36). As a matter of fact, if we make a transparent overlay of Fig. 12(a) and 12(b), the resulting figure would be identical to Fig. 4, which shows the basic geometry for four-wave mixing.

Having established the formal analogy between real-time four-wave mixing and holography, it is natural to explore the possibility of applying four-wave mixing to some applications for which conventional holography has been considered. At Caltech we analyzed the possibility of performing spatial convolution and correlation [17]. In conventional holography, one performs spatial filtering, convolution, and correlation in the focal plane of suitably placed lenses [18]. It is thus natural to extend the same line of reasoning to nonlinear experiments in which the photographic film of holography is replaced by a nonlinear optical medium. It is very gratifying to find that this wedding of nonlinear optics and Fourier optics preserves the formal mathematical elegance of both disciplines. As an extra bonus, the results suggest the possibility of useful applications.

Consider the nature of the resultant field produced as a result of the simultaneous mixing of three optical fields, all of radian frequency ω, incident upon a thin medium possessing a third-order nonlinear optical susceptibility $\chi_{NL}^{(3)}$ centered at the common focal plane of two identical lenses (or mirrors) of focal length f. The geometry is illustrated in Fig. 13. Each field is specified spatially at the front focal plane of its respective lens with the following amplitudes:

$$\begin{aligned} E_1 &= \tfrac{1}{2} A_1(x,y,z) \exp i(kz - \omega t) + \text{c.c.} \\ E_2 &= \tfrac{1}{2} A_2(x,y,z) \exp -i(kz + \omega t) + \text{c.c.} \\ E_4 &= \tfrac{1}{2} A_4(x,y,z) \exp i(kz - \omega t) + \text{c.c.} \end{aligned} \tag{37}$$

where $A_{1,4}(x,y,0) \equiv u_{1,4}(x,y)$, and $A_2(x,y,4f) \equiv u_2(x,y)$. Fields E_1 and E_2 are essentially counterpropagating, with E_4 being parallel to these fields and separated either spatially [e.g., shifted by (x_s, y_s)] or via orthogonal polarizations. The

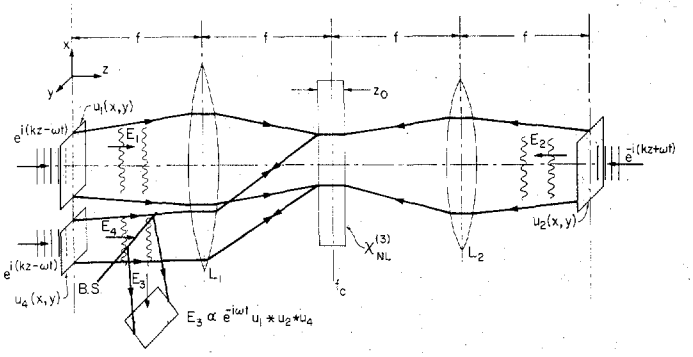

Fig. 13. Convolution/correlation geometry. All input optical fields are at frequency ω. *BS* is a beam splitter necessary to view the desired output E_3 which is evaluated at a plane located a distance f from the lens L_1.

u_i contain the input information to be convolved or correlated, which can, for example, be in the form of phase and/or amplitude transparencies. The u_i are assumed to be illuminated by plane waves, all of the same frequency ω.

After propagating through lens L_1, A_1 has the following form (in the Fresnel approximation)

$$A_1(x,y;f\leqslant z\leqslant 3f)=\frac{\exp ikn\Delta\exp ikz}{i\lambda f}\times\mathcal{F}\left[u_1(x',y')\exp\frac{ik}{2f}\left(2-\frac{z}{f}\right)\cdot(x'^2+y'^2)\right]_{f_x=\frac{x}{\lambda f};f_y=\frac{y}{\lambda f}}$$

where $\mathcal{F}[a]\equiv\tilde{a}$ is the Fourier transform of a, and

$$h=\exp ikn\Delta\exp-\frac{ik}{2f}(x^2+y^2) \tag{39}$$

is the transmission function of a thin lens [18]. Similarly, the complex amplitude of E_2 has the form (after propagating through lens L_2)

$$A_2(x,y;f\leqslant z\leqslant 3f)=\frac{\exp ikn\Delta\exp ik(4f-z)}{i\lambda f}\times\left\{\mathcal{F}\left[u_2(x',y')\exp-\frac{ik}{2f}\;2-\frac{z}{f}\cdot(x'^2+y'^2)\right]_{f_x=\frac{x}{\lambda f};f_y=\frac{y}{\lambda f}}\right.$$

Anticipating the mixing process of interest, we express the complex conjugate amplitude of E_4 (after propagating through lens L_1) as

$$A_4^*(x,y;f\leqslant z\leqslant 3f)=\frac{\exp-ikn\Delta\exp-ikz}{-i\lambda f}\times\left\{\mathcal{F}\left[u_4(x',y')\exp\frac{ik}{2f}\left(2-\frac{z}{f}\right)\cdot(x'^2+y'^2)\right]_{f_x=\frac{x}{\lambda f};f_y=\frac{y}{\lambda f}}\right\}^* \tag{41}$$

The fields A_i in (38), (40), and (41) become directly proportional to the Fourier transforms of their respective u_i if the terms inside the square brackets in the exponents can be neglected. This happens when

$$|z-2f|\ll\frac{2f^2\lambda}{r_i^2} \tag{42}$$

where r_i is the spatial extent of u_i.

We now place a medium centered at the focal plane f_c of thickness z_0 [satisfying the constraint (42)] which possesses a third-order nonlinear optical susceptibility $\chi^{(3)}_{NL}$. Without loss of generality, we assume a transparent, lossless medium, and neglect linear refractive effects.

The complex amplitude of nonlinear polarization at $\omega=\omega+\omega-\omega$ generated by the mixing of the three waves is of the form (33)

$$P_{NL_i}=\chi^{(3)}_{ijkl}A_{1_j}A_{2_k}A^*_{4_l} \tag{43}$$

where repeated indices are summed over the field polarizations. The resultant radiated field E_3 is given by

$$A_3(\bar{x})=-\frac{4\pi\omega^2}{c^2}\int P_{NL}(\bar{x}')\,G(\bar{x},\bar{x}')\,d^3\bar{x}' \tag{44}$$

where

$$G(\bar{x},\bar{x}')=-\frac{1}{4\pi}\frac{e^{ikr}}{r} \tag{45}$$

is the Green's function that satisfies the wave equation. Using (38), (40), and (41) in (43) and (44), as well as condition (42), integrating over the volume of the nonlinear medium, and "propagating" back to $z=0$ through lens L_1, we get (after a very elaborate manipulation)

$$A_3(x_0,y_0,0)=-i\frac{2\pi\omega}{c}\frac{z_0}{\lambda^4f^4}\exp 2ikn\Delta\exp 4ikf\cdot\mathcal{F}\left[\tilde{u}_1(x,y)\,\tilde{u}_2(x,y)\,\tilde{u}_4^*(x,y)\cdot\chi^{(3)}_{NL}(x,y)\right]_{f_x=\frac{x_0}{\lambda f};f_y=\frac{y_0}{\lambda f}} \tag{46}$$

where $\chi^{(3)}_{NL}(x,y)$ is the proper tensor element in (43) connecting fields 1, 2, 3, and 4.

If $\chi^{(3)}_{NL}$ is spatially homogeneous, the output field becomes

$$A_3(x_0,y_0,0)=\psi u_1(-x,-y)*u_2(-x,-y)\star u_4(-x,-y) \tag{47}$$

where

$$\psi=-i\frac{2\pi\omega}{c}\frac{z_0}{\lambda^4f^4}\exp 2ikn\Delta\exp 4ikf\,\chi^{(3)}_{NL}. \tag{48}$$

In (47) the symbols $*$ and $\star$ denote the standard operations of convolution and correlation, respectively [18].

Equation (47) is our primary result. We obtain the spatial convolution of u_1 and u_2 by taking u_4 as a point source. This leads to

$$A_3(x_0,y_0,0)=\psi u_1*u_2. \tag{49}$$

Similarly, the correlation operation is performed by placing information on fields u_1 and u_4, with a point source for u_2 yielding

$$A_3(x_0, y_0, 0) = \psi u_1 \star u_4, \tag{50}$$

where the u_i in (49) and (50) are the inverted images of the input fields.

The correlation of u_2 and u_4 is similarly obtained by using a point source for u_1. For Gaussian beams (which will be discussed below), the finite spot size in the focal plane (f_c) of the "point source" input will ultimately limit the spatial frequency bandwidth of the above operations.

We can now appreciate the advantage of using a degenerate four-wave mixing approach to real-time operations. The third field (which corresponds to the point source input mentioned above) provides an optical carrier frequency upon which the convolution or correlation information is placed. No frequency scaling factors are present, the entire system requires only a single frequency source, and within the Fresnel approximation the phase matching condition is satisfied. Finally, the "degenerate" operations of autoconvolution and autocorrelation can be performed with a single optical frequency.

The approximations used in the above discussion place upper limits on both the resolution (or spatial frequency bandwidth), and the efficiency (or nonlinear gain) of the interaction. The Fresnel approximation is related to $f_{\max}$, the greatest spatial frequency present, by

$$f_{\max} < \left(\frac{4}{\pi\lambda^3 f}\right)^{1/4}. \tag{51}$$

This same approximation also places an upper limit on the input field spot size, which is given by

$$d < \left(\frac{4\lambda f^3}{\pi}\right)^{1/4}. \tag{52}$$

Hence the maximum number of resolution elements possible is derivable through (51) and (52), yielding

$$N_{\max} = \frac{16f}{\pi\lambda}. \tag{53}$$

Using values of 10 cm and 0.5 for f and λ, respectively, leads to a value of 10^3 cm^{-1} for $f_{\max}$, which corresponds to a grid of 1000×1000 resolution elements. Therefore, since the phase matching condition is satisfied for all the field momentum components in the Fresnel approximation, this technique can be useful for complex spatial information processing.

VII. Phase Conjugation by Stimulated Brillouin Scattering

The first demonstration of distortion correction by nonlinear optical techniques was reported by Zeldovich *et al.* [1] and Nosach *et al.* [2]. The reported experiment used a ruby laser beam, which was distorted by passing through a roughened plate of glass, as a pump for stimulated Brillouin scattering in pressurized methane gas. The backward propagating stimulated beam passed in reverse through the distorting plate and emerged from it with an undistorted wavefront similar to that of the pumping beam before impinging on the distorting plate. The experimental setup is shown in Fig. 14.

A similar experiment was performed by Wang and Giuliano [12] who verified the distortion compensation by accurate measurements of the beam divergence before and after the compensation. The results of this experiment are shown in Fig. 15.

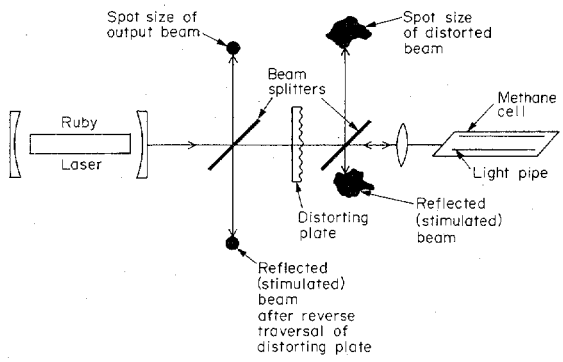

Fig. 14. Experimental setup used by Zeldovich *et al.* [1] for correction of phase distortion by stimulated Brillouin scattering.

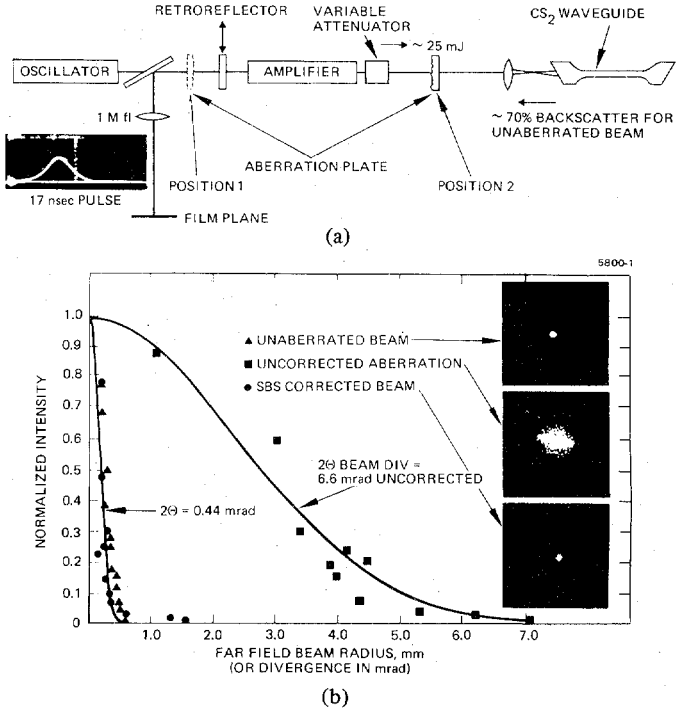

Fig. 15. (a) The experimental setup in the experiment of Wang and Giuliano. (b) A radial intensity plot of the uncorrected and corrected beam.

In this experiment, the phase conjugation occurs in the process of stimulation with the distorted beam acting as a pump. The process involves a threshold phenomenon and the explanation of why the stimulated and reflected beam are conjugated is more subtle than that of the direct three- and four-wave mixing schemes described.

The basic explanation which was advanced by Zeldovich *et al.* [1] is that the phase conjugate replica of the pump wave is the field configuration which exercises the *largest* spatial gain coefficient and is thus favored in the stimulation process.

The theoretical proof of this last statement proceeds as follows. Consider the wave equation obeyed by the backward propagating "signal" beam

$$E_s(r_\perp, z) = \mathcal{E}_s(r_\perp, z) \exp ik_s z \tag{54}$$

where the time factor exp ($i\omega_{st}$) is omitted. The field obeys the wave equation

$$\nabla^2 E_s(r_\perp, z) + \omega_s^2 \mu\epsilon E_s = \mu \frac{\partial^2}{\partial t^2} P_{NL} \tag{55}$$

where P_{NL} accounts for the acoustooptic interaction with the laser pump wave.

Using (54) in (55), recognizing that $k_s^2 = \omega_s^2 \mu\epsilon$, assuming $|\partial^2 \mathcal{E}_s/\partial z^2| \ll |k_s(\partial \mathcal{E}_s/\partial z)|$, $|k_s^2 \mathcal{E}_s|$, and defining $\nabla_t^2 = (\partial^2/\partial x^2) + (\partial^2/\partial y^2)$, leads to

$$\frac{\partial \mathcal{E}_s}{\partial z} + \frac{i}{2k_s} \nabla_t^2 \mathcal{E}_s + \frac{1}{2} g(r_\perp, z)\, \mathcal{E}_s = 0 \tag{56}$$

where $g(r_\perp, z)$ is the local gain exercised by the signal wave due to stimulated Brillouin interaction with the pump wave

$$\mathcal{E}_L(r_\perp, z) \exp -ik_L z.$$

Under conditions of very short phonon lifetimes, the gain g can be shown to be proportional to the pump intensity

$$g(r_\perp, z) = A\, |E_L(r_\perp, z)|^2 \tag{57}$$

where A is given by

$$A = \frac{\pi^2 p^2 \epsilon_0 n^8}{\alpha \rho v^2 \lambda^2} \tag{58}$$

and where λ is the laser wavelength, p = photoelastic coefficient, n is the index of refraction, α the sound (intensity) absorption coefficient (at the frequency $\nu_{\text{sound}} = (2n\nu/c)v$), ρ the material mass density, and v the velocity of sound in the medium.

If we neglect the depletion of the laser intensity and the losses at the laser frequency, then the laser field

$$E_L(r_\perp, z) = \mathcal{E}_L(r_\perp, z) \exp - ik_L z \tag{59}$$

obeys

$$\frac{\partial \mathcal{E}_L}{\partial z} - \frac{i}{2k_L} \nabla_t^2 \mathcal{E}_L = 0. \tag{60}$$

We note that since $k_s - k_L \simeq 10^{-5} k_L$, we will assume in the following $k_s \simeq k_L \equiv k$.

Consider a system of functions $f_k(r_\perp, z)$ such that

$$\frac{\partial f_k}{\partial z} + \frac{i}{2k} \nabla_t^2 f_k = 0 \tag{61}$$

and

$$\int f_i^*(r_\perp, z)\, f_k(r_\perp, z)\, dr_\perp = \delta_{ik}. \tag{62}$$

Choose the function f_0^* such that it coincides within a constant B with the laser field

$$\mathcal{E}_L(r_\perp, z) = B f_0^*(r_\perp, z). \tag{63}$$

The remaining members of the set f_k are generated starting from the orthogonality relation (62). The sought field $\mathcal{E}_s(r_\perp, z)$ is expanded in the form of

$$\mathcal{E}_s(r_\perp, z) = \sum_{k=0}^{\infty} C_k(z) f_k(r_\perp, z). \tag{64}$$

Substituting (58) in (50) yields

$$\sum_k \frac{dC_k}{dz} f_k + C_k \frac{\partial f_k}{\partial z} + i \frac{C_k}{2k} \nabla_t^2 f_k + \frac{1}{2} AB^2 |f_0|^2 C_k f_k = 0. \tag{65}$$

The sum of the second and third terms is zero in virtue of (61). We next multiply (65) by $\int dr\, f_i^*(r_\perp, z)$ which, using (62), leads to

$$\frac{dC_i}{dz} + \frac{1}{2} \sum_{k=0}^{\infty} g_{ik}(z)\, C_k(z) = 0 \tag{66}$$

with

$$g_{ik}(z) = AB^2 \int dr_\perp |f_0(r_\perp, z)|^2 f_i^*(r_\perp, z) f_k(r_\perp, z). \tag{67}$$

If the intensity $|f_0(r_\perp, z)|^2$ of the laser field fluctuates strongly as a function of $r_\perp$, then it follows from (67) that in general the partial overlap of maxima and minima of $|f_0(r_\perp, z)|^2$ and $f_i^*(r_\perp, z) f_k(r_\perp, z)$ as well as the complex nature of these functions will cause g_{ik} to be a small number except for g_{oo}, since

$$g_{oo} = AB^2 \int dr_\perp |f_0(r_\perp, z)|^4 \tag{68}$$

and no cancellation occurs. It follows that under these conditions the coefficient C_0 grows (with distance) more rapidly than the other C_i so that after a sufficient distance, the field $\mathcal{E}_s$ is given according to (64)

$$\mathcal{E}_s(r_\perp, z) = \sum_{k=0}^{\infty} C_k(z) f_k(r_\perp, z) \simeq C_0(z)\, f_0(r_\perp, z)$$

$$= \frac{C_0(z)}{B^*}\, \mathcal{E}_L^*(z) \tag{69}$$

i.e., the *Stokes field generated by stimulated Brillouin (back) scattering is the complex conjugate of the incident laser field* and is thus in the proper form to correct in its backward travel for the phase distortions undergone by the laser field.

We note that if $f_0(r_\perp, z)$ is not a strongly fluctuating function of $r_\perp$ then g_{oo} and g_{ii} will be of the same order of magnitude and the preferential growth of C_0, which leads to phase conjugation, will not take place. The introduction of additional phase aberration in front of the Brillouin cell may thus improve the phase conjugation.

In the above derivation, no initial boundary for $C_i(z)$ was specified, since no input exists. It is assumed that the input fields are due to zero point vibrations of the electromagnetic field at the Stokes' frequency.

Before concluding it may be useful to review some of the main directions and possibilities which are already evident in this new field.

The work of Zeldovich *et al.* [1] points the way toward using phase conjugation techniques including stimulated Brillouin and Raman scattering in real time for the correction of distortion in the *atmosphere* and in *passive* and *active* optical components. These may be especially important in high power lasers where the optical integrity of wavefronts is a problem of serious concern. Phase conjugators incorporated into high power laser oscillators can yield the full available power in the form of a diffraction limited beam. In the case of satellite communication through the atmosphere, we can envisage a weak probing beam transmitted from a satellite to earth through the atmosphere. The beam is conjugated, amplified to the requisite power level, and retransmitted through the atmosphere, reaching the satellite as a diffraction limited spot size.

A second class of applications [16], [17] involves the use of

phase conjugation for real-time holographic applications. These include image transmission through fibers, as well as convolution and correlation as discussed above. In these cases, it will be important to perform these experiments on a CW basis with moderate power levels. One approach in this direction was demonstrated by Bloom, Liao, and Economou [9] who demonstrated four-wave phase conjugation using the resonantly enhanced Kerr nonlinearity of atomic sodium vapor [19]. Another approach is to use multimode optical waveguides, solid or filled with some suitable fluid, as the medium for wave conjugation. An analysis of this possibility [20] shows that all the main features of the bulk interaction are preserved in the case of fibers. The number of resolution elements in the pictorial field cannot exceed the number of guided modes in the fiber. Due to the large intensities which result in small diameter (10-100 μm) fibers and the confinement of the radiation over large lengths, CW phase conjugation with power levels of $\sim$1 W are estimated.

The amplification property of the transmitted or reflected wave can be used in image amplification. By using simultaneously a number of pump waves of different wavelengths, we should be able to achieve amplification of color images.

To summarize: Phase conjugation by nonlinear techniques has been shown formally to be analogous to holography. This, in combination with the added features of real-time operation, amplification, and oscillation, promises the potential of many new and interesting applications involving the processing and restoration of optical wave fronts.

Acknowledgment

I would like to express my appreciation to my colleagues and students who participated with me in developing these ideas: V. Wang, R. L. Abrams, and V. Evtuhov at the Hughes Research Laboratories, Malibu, and P. Yeh, D. Fekete, J. AuYeung, and D. M. Pepper at the California Institute of Technology.

References

[1] B. Y. Zeldovich, V. I. Popovichev, V. V. Ragulskii, and F. S. Faisullov, "Connection between the wave fronts of the reflected and exciting light in stimulated Mandel'shtam-Brillouin scattering," *Sov. Phys.–JETP*, vol. 15, p. 109, 1972.

[2] O. Y. Nosach, V. I. Popovichev, V. V. Ragulskii, and F. S. Faisullov, *Sov. Phys.–JETP*, vol. 16, p. 435, 1972.

[3] A. Yariv, "Three-dimensional pictorial transmission in optical fibers," *Appl. Phys. Lett.*, vol. 28, p. 88, 1976.

[4] A. Yariv, "On transmission and recovery of three-dimensional image information in optical waveguides," *J. Opt. Soc. Amer.*, vol. 66, p. 301, 1976.

[5] R. W. Hellwarth, "Generation of time reversal wavefronts by nonlinear refraction," *J. Opt. Soc. Amer.*, vol. 67, p. 1, 1977.

[6] A. Yariv and D. M. Pepper, "Amplified reflection, phase conjugation, and oscillation in degenerate four-wave mixing," *Opt. Lett.*, vol. 1, p. 16, 1977.

[7] S. L. Jensen and R. W. Hellwarth, "Observation of the time-reversed replica of a monochromatic optical wave," *Appl. Phys. Lett.*, vol. 32, p. 166, 1978.

[8] D. M. Bloom and G. E. Bjorklund, "Conjugate wave front generation and image reconstruction by four-wave mixing," *Appl. Phys. Lett.*, vol. 31, p. 592, 1977.

[9] D. M. Bloom, P. F. Liao, and N. P. Economu, "Observation of amplified reflection by degenerate four-wave mixing in atomic sodium vapor," *Opt. Lett.*, vol. 2, p. 158, 1978.

[10] D. M. Pepper, D. Fekete, and A. Yariv, *Appl. Phys. Lett.*, to be published.

[11] P. V. Avizonis, F. A. Hopf, W. D. Bamberger, S. F. Jacobs, A. Tomita, and K. H. Womack, "Optical phase conjugation in a lithium-niobate crystal," *Appl. Phys. Lett.*, vol. 31, p. 435, 1977.

[12] V. Wang and C. R. Giuliano, "Correction of phase aberrations via stimulated Brillouin scattering," presented at the 1977 IEEE OSA Conf. Laser Engineering and Applications, Washington, DC, June 1977, Paper 17.6; also, *Opt. Lett.*, vol. 2, p. 4, 1978.

[13] B. Ya Zeldovich and V. V. Shkunov, "Wavefront reproduction in stimulated Raman scattering," *Sov. J. Quantum Electron.* (English transl.), vol. 7, p. 610, 1977.

[14] See, for example, R. W. Minck, R. W. Terhune, and C. C. Wang, "Nonlinear optics," *Appl. Opt.*, vol. 5, p. 1595, 1966; or A. Yariv, *Quantum Electronics*, 2nd ed. New York: Wiley, 1975.

[15] S. E. Harris, "Proposed backward wave oscillation in the infrared," *Appl. Phys. Lett.*, vol. 9, p. 114, 1966.

[16] A. Yariv, "Four-wave mixing as real time holography," *Opt. Commun.*, to be published.

[17] D. M. Pepper, J. AuYeung, D. Fekete, and A. Yariv, "Spatial convolution and correlation of optical fields via degenerate four-wave mixing," *Opt. Lett.*, to be published.

[18] J. W. Goodman, *Introduction to Fourier Optics*. New York: McGraw-Hill, 1968.

[19] R. L. Abrams and R. C. Lind, "Degenerate four-wave mixing in absorbing media," *Opt. Lett.*, vol. 2, p. 94, 1978.

[20] A. Yariv, J. AuYeung, D. Fekete, and D. M. Pepper, "Image phase compensation by four-wave mixing in optical fibers," *Appl. Phys. Lett.*, vol. 32, p. 635, 1978.